Electronic Supplementary Material (ESI) for Journal of Materials Chemistry A.
This journal is © The Royal Society of Chemistry 2017

Supplementary Information

Direct growth of Ternary Ni-Fe-P Porous Nanorods onto nickel foam as a Highly Active, Robust Bi-functional Electrocatalyst for Overall Water Splitting

*Sung Hoon Ahn and Arumugam Manthiram**

Materials Science and Engineering Program & Texas Materials Institute

The University of Texas at Austin, Austin, Texas, 78712, United States

Corresponding Author

E–mail: manth@austin.utexas.edu

Experimental Section

Preparation of MOF-derived porous Ni-Fe-P nanorods

Synthesis of $Ni_{0.7}Fe_{0.3}$ oxyhydroxide nanoflakes on nickel foam: The commercial nickel foam was successively cleaned with ethanol, acetone, and ethanol for 30 min each. The growth solution was prepared by dissolving 0.07 M nickel nitrate hexahydrate, 0.03 M Iron(III) nitrate nonahydrate, and 0.25 M urea in 20 mL of deionized water. Four pieces of nickel foam (1 X 4 cm) were submersed in the above solution, and $Ni_{0.7}Fe_{0.3}$ oxyhydroxide nanoflakes (NiFe NFs) were directly grown onto the commercial nickel foam at 100 ^{o}C for 3 h in an electric oven. The resulting NiFe NFs were washed with ethanol twice and dried in a vacuum oven at 50 ^{o}C overnight.

Synthesis of Ni-Fe MOF nanorods on nickel foam: 400 mg of 2,5-Dihydroxyterephthalic acid(H4DOBDC) was dissolved in 80 mL dimethylformamide(DMF), and the resulting solution was transferred into a 100-mL Teflon-lined stainless-steel autoclave. 10 pieces of the NiFe NFs on the nickel foam were submersed into the above solution, heated at 155 ^{o}C for 12 h in an electric oven, and then cooled down to room temperature naturally. The resulting Ni-Fe MOF nanorods (Ni-Fe MOF-NRs) were washed with ethanol twice and dried in a vacuum oven at 50 ^{o}C overnight.

Synthesis of Ni-Fe-P porous nanorods on nickel foam: Ni-Fe MOF NRs on nickel foam were loaded onto a graphite box and then placed into tubular furnace. 1 g of sodium hypophosphite monohydrate (NaH_2PO_2) was loaded onto a graphite box placed on the upstream side of the argon flow in the tubular furnace. The Ni-Fe-P porous nanorods (Ni-Fe-P porous NRs) on nickel foam were obtained after phosphidation at 300 ^oC for 1 h with a ramping rate of 5 ^oC min^{-1} under argon flow.

Synthesis of $Ni_{0.3}Fe_{0.7}$ oxyhydroxide nanoflakes on nickel foam: The same procedure with $Ni_{0.7}Fe_{0.3}$ oxyhydroxide nanoflakes was conducted except for the preparation of the growth solution. The growth solution for $Ni_{0.3}Fe_{0.7}$ oxyhydroxide nanoflakes was prepared by dissolving 0.03 M nickel nitrate hexahydrate, 0.07 M Iron(III) nitrate nonahydrate, and 0.25 M urea in 20 mL of deionized water.

Synthesis of Ni oxyhydroxide nanoflakes on nickel foam: The same procedure with $Ni_{0.7}Fe_{0.3}$ oxyhydroxide nanoflakes was conducted except for the preparation of the growth solution. The growth solution for Ni oxyhydroxide nanoflakes was prepared by dissolving 0.1 M nickel nitrate hexahydrate and 0.25 M urea in 20 mL of deionized water.

Synthesis of NiCo oxyhydroxide nanoflakes on nickel foam: The same procedure with $Ni_{0.7}Fe_{0.3}$ oxyhydroxide nanoflakes was conducted except for the preparation of the growth solution. The growth solution for $Ni_{0.7}Co_{0.3}$ oxyhydroxide nanoflakes was prepared by dissolving 0.07 M nickel nitrate hexahydrate, 0.03 M Cobalt(II) nitrate hexahydrate, and 0.25 M urea in 20 mL of deionized water.

Electrochemical measurements

Electrochemical analysis was performed with a potentiostat (Autolab PGSTAT302N) and a conventional three-electrode configuration with Ni-Fe based catalyst on nickel foam as a working electrode, platinum mesh as a counter electrode, and saturated chalome electrode (SCE) as a reference electrode. The potential versus reversible hydrogen electrode (E_{RHE}) is converted from potential versus SCE (E_{SCE}) following the Nernst equation:

$$E_{RHE} = E_{SCE} + 0.059 \times (pH) + 0.242 \quad (1)$$

The linear sweep voltammetry (LSV) curves were obtained in N_2 saturated 1 M KOH solution at 0.25 mV s^{-1}. The stability of the catalysts was evaluated by chronopotentiometry analysis at 10 mA cm^{-2} for 24 h. The electrochemical surface area (ECSA) was determined by measuring

the capacitive current associated with the double-layer charging from the scan rate dependence of cyclic voltammetry (CV). The CVs were recorded in the potential range between 1.3 and 1.4 E_{RHE} at the scan rates with 5, 10, 25, 50, 100, 200, 400, 600, 800 and 1,000 mV s^{-1}. The double-layer capacitance (C_{dl}) was estimated by plotting the current density variation, $\Delta J = (J_a - J_c)$ at 1.35 E_{RHE}. The linear slope is twice of the double-layer capacitance. The produced hydrogen and oxygen were sampled by a gas-tight syringe and measured by a gas chromatograph (GC) equipped with a thermal conduction detector (Shimadzu).

Physical Characterizations:

Scanning electron microscopy (SEM) images were obtained with a FEI Quanta 650 SEM equipped with energy dispersive spectroscopy (EDX). Transmission electron microscopy (TEM) and high resolution TEM (HRTEM) images and element mapping analysis were conducted on a JEOL 2010F TEM. X-ray photoelectron spectroscopy (XPS) analysis was performed on a Kratos Axis Ultra DLD spectrometer with a monochromatic Al (Kα) radiation source (1486.6 eV). X-ray diffraction (XRD) patterns were collected with a Rigaku MiniFlex 600 diffractometer operating with Cu Kα source, with a step size of 0.05° and a scan range between 10° and 80°.

N_2 adsorption-desorption isotherms and pore-size distributions were determined at 77 K with a Quantachrome AutoSorb iQ2 instrument. The specific surface area was calculated from N_2 adsorption−desorption isotherm applying the Brunauer − Emmett – Teller (BET) model. The pore volume and pore size distribution were also calculated from the nitrogen isotherm using the Barrett – Joyner - Halenda (BJH) model.

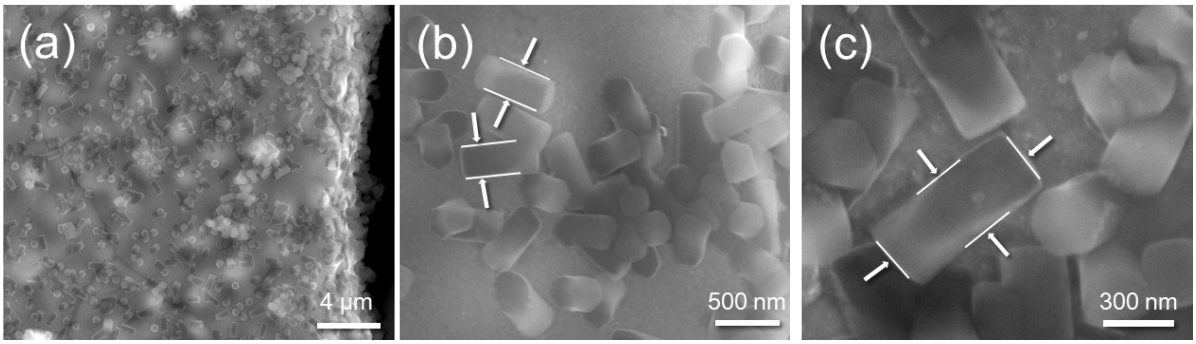

Fig. S1 FE-SEM images of the NiFe MOF NRs converted from the NiFe NFs grown at 100 °C for 1 h. The areal density of the nanorods on nickel foam is lower than that on the counterpart converted from the NiFe NFs grown at 100 °C for 3 h, which is a typical

synthesis condition, while the shape and size of the MOF nanorods are identical.

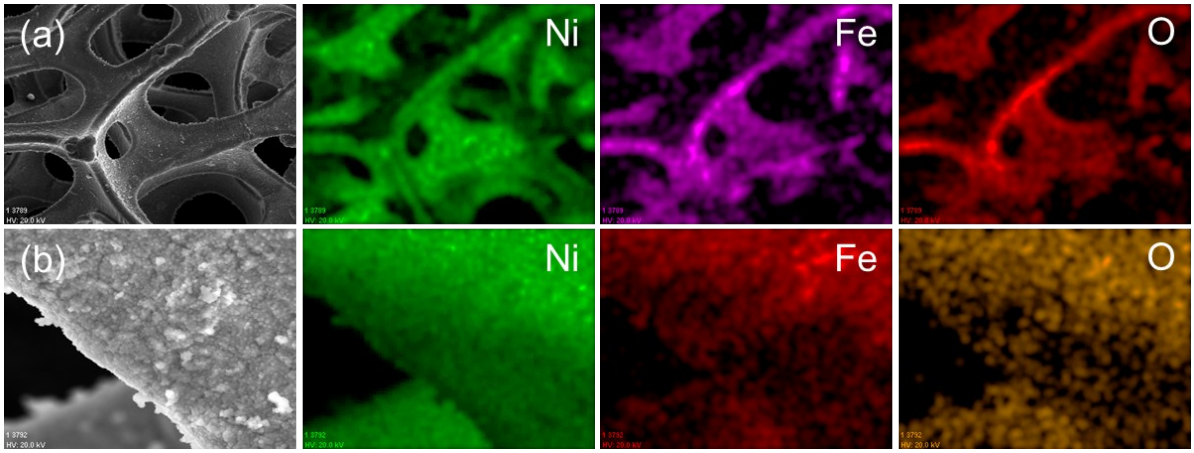

Fig. S2 FE-SEM images of NiFe MOF NRs at (a) low- and (b) high-resolution and elemental mapping for Ni, Fe, and O.

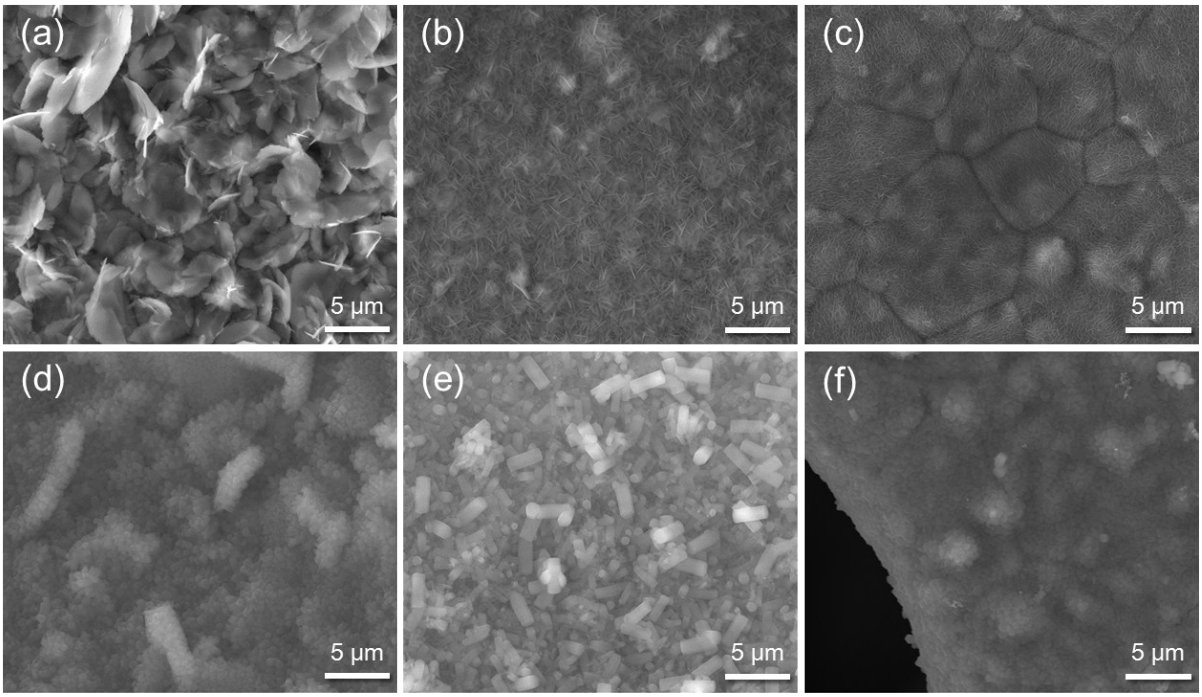

Fig.S3 FE-SEM images of (a) micrometer-size $Ni_{0.3}Fe_{0.7}$ hydroxide nanosheets, (b) nickel hydroxide nanoflakes, and (c) $Ni_{0.7}Co_{0.3}$ hydroxide nanoflakes and the corresponding samples after MOF-treatment for (d) micrometer-size NiFe, (e) Ni, and (f) NiCo.

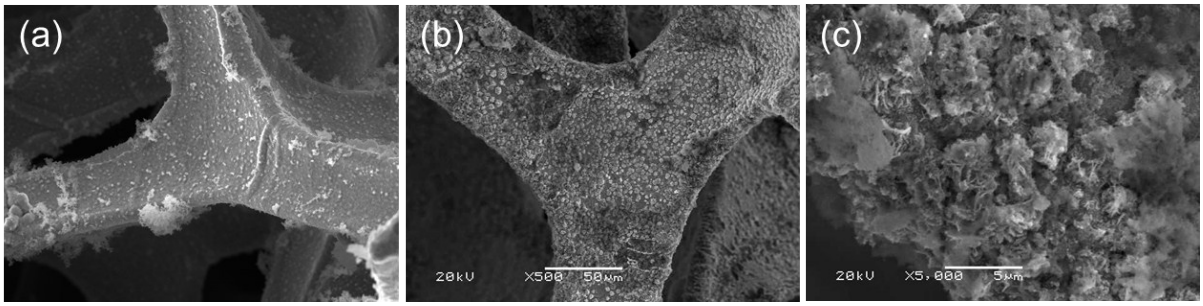

Fig. S4 SEM image of (a) NiFe NFs, and (b) low-, and (c) high-resolution SEM images of Ni-Fe-P after phosphidation without MOF treatment.

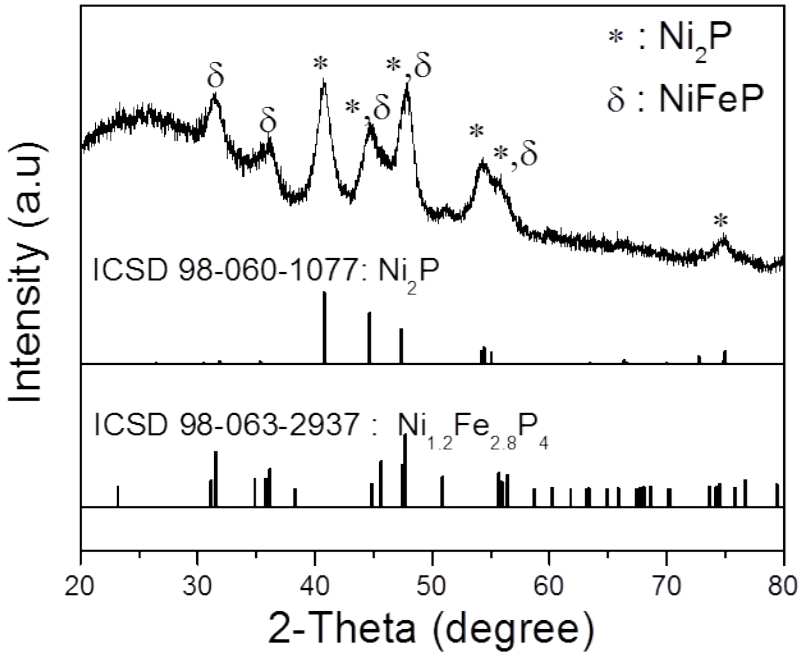

Fig.S5 XRD patterns of porous Ni-Fe-P nanorods.

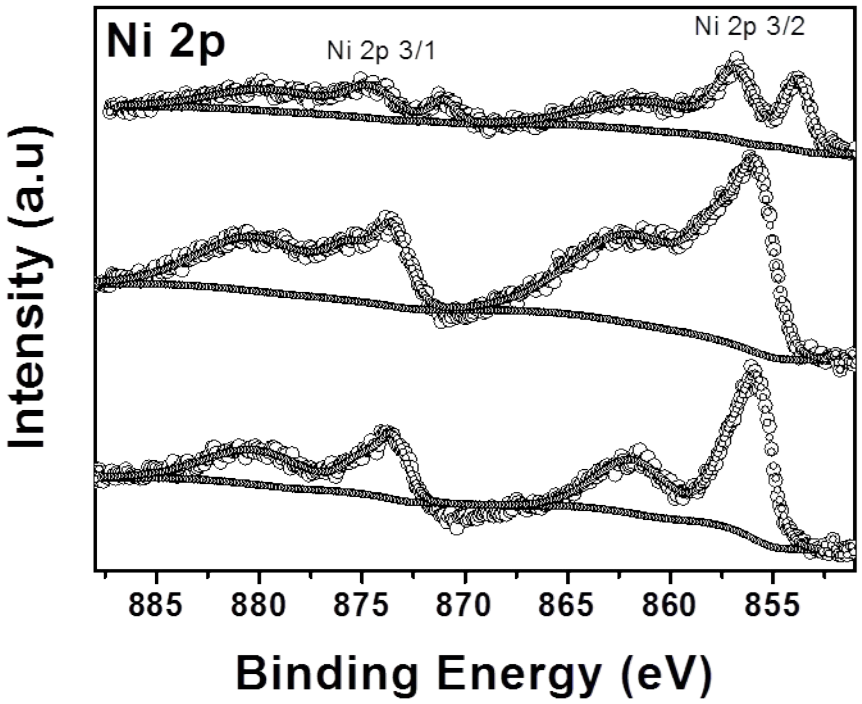

Fig.S6 High resolution XPS Ni 2p spectra of Ni-Fe-P@C NRs.

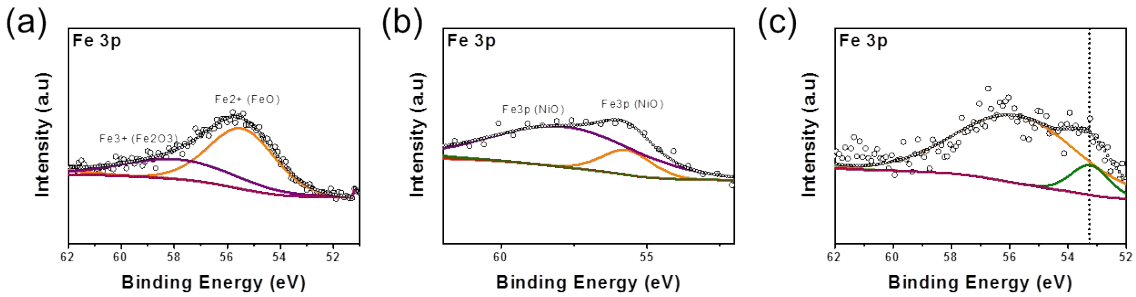

Fig. S7 High resolution Fe 3p XPS spectra of (a) NiFe NFs, (b) Ni-Fe MOF NRs, and (c) porous Ni-Fe phosphide NRs.

.

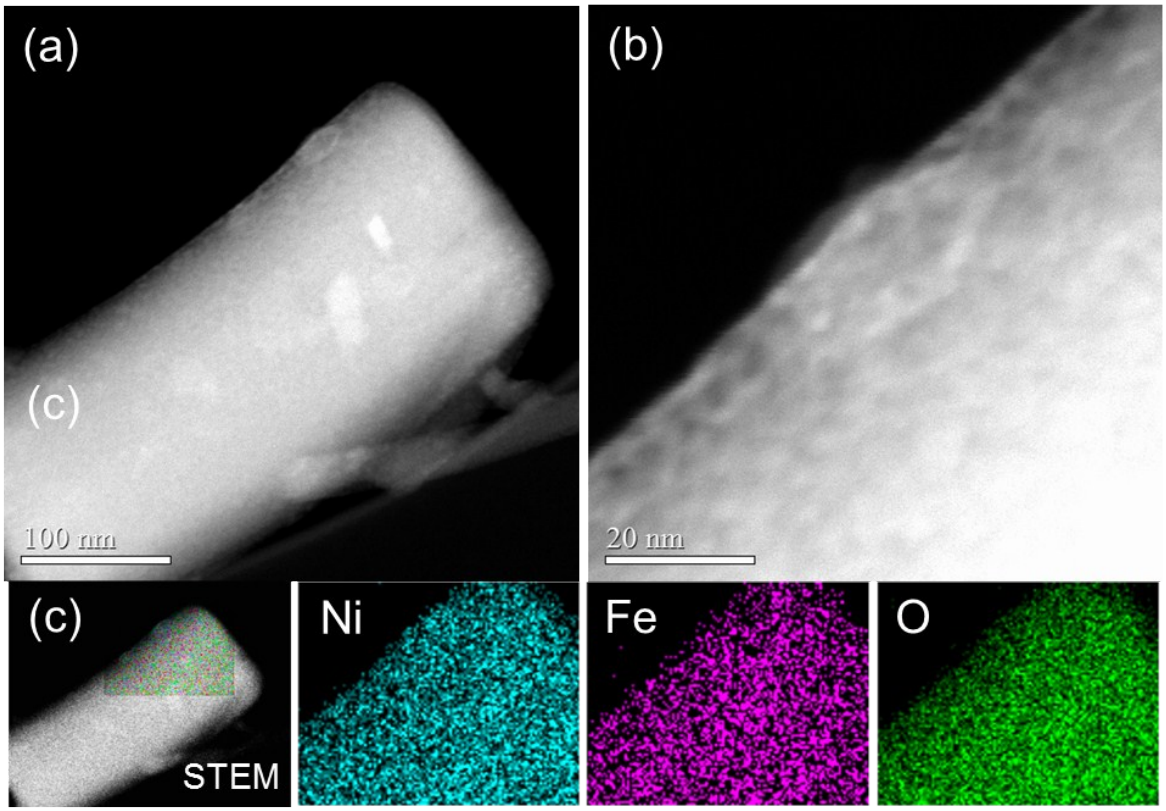

Fig. S8 (a) Low-, and (b) high-resolution STEM images of Ni-Fe MOF nanorod and the corresponding EDX mappings for Ni, Fe and O.

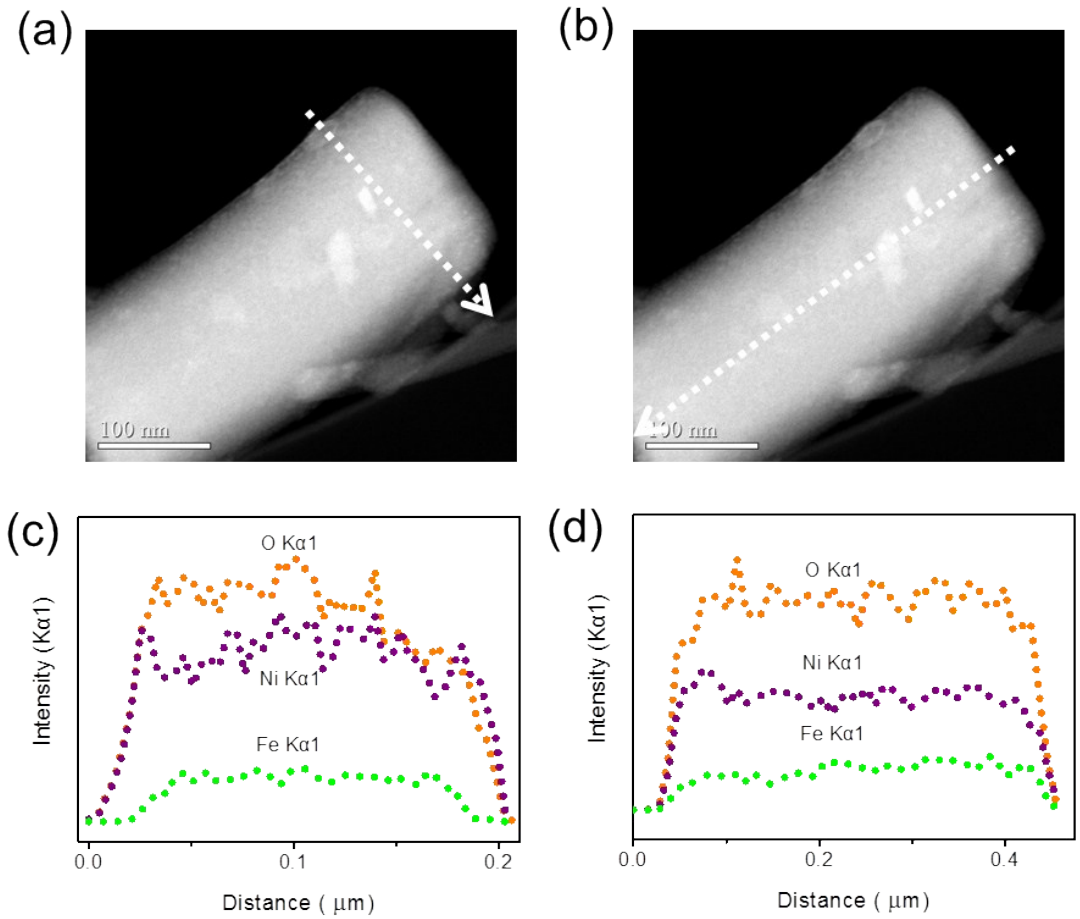

Fig.S9 STEM images of Ni-Fe MOF nanorod and the corresponding EDX line scanning for Ni, Fe and O.

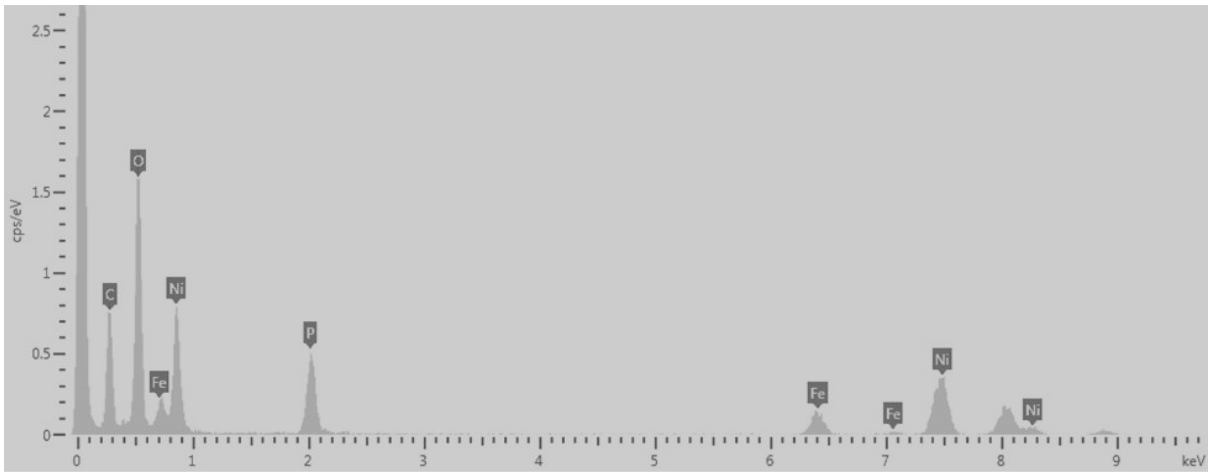

Map Sum Spectrum	Atomic %
Ni	7.24
Fe	2.73
P	9.19
O	56.77
C	24.07
Total	100.00

Fig. S10 EDX spectrum of porous Ni-Fe-P nanorods.

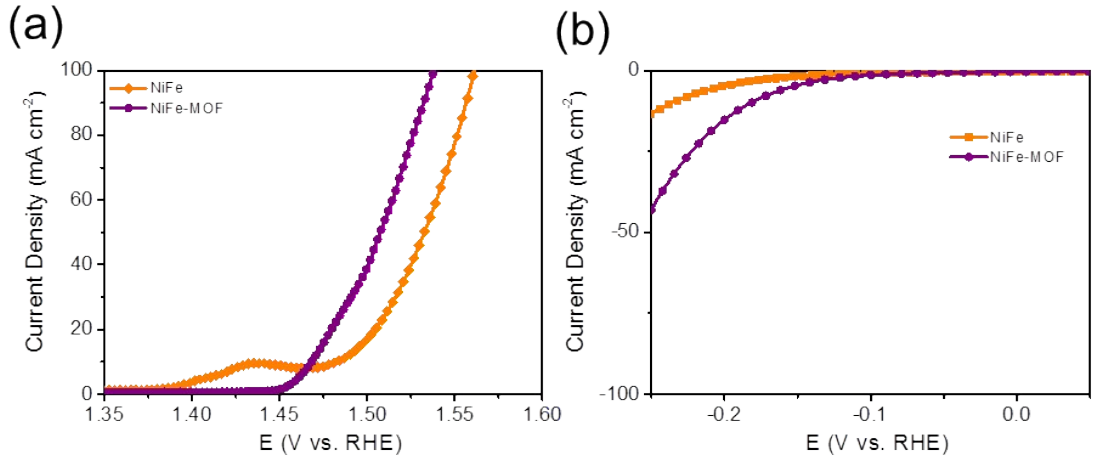

Fig. S11 Linear sweep voltammetry (LSV) curves of MOF treated Ni-Fe nanorods toward (a) OER and (b) HER in N_2-saturated 1 M KOH solution at 1 mV s^{-1}.

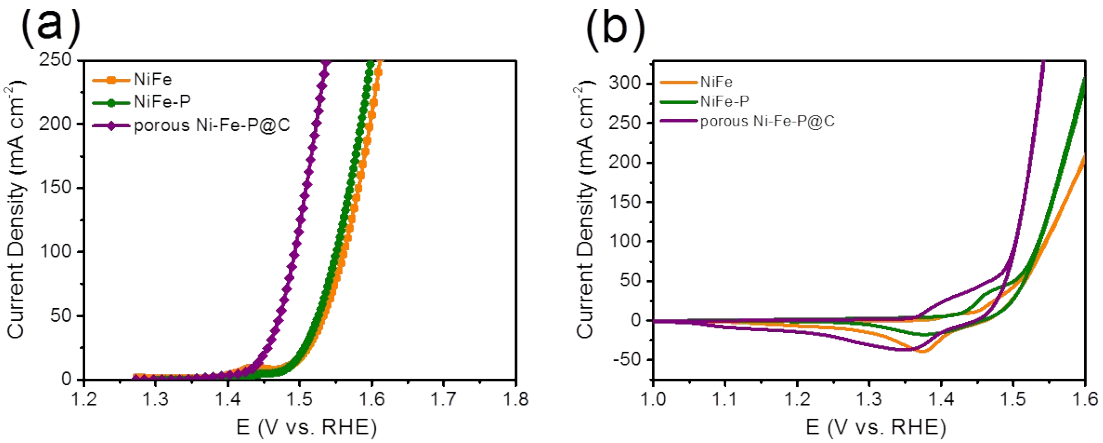

Fig. S12 (a) LSV curves of NiFe NFs, Ni-Fe-P, and porous Ni-Fe-P@C NRs on nickel foam. (b) Cycling voltammetry (CV) with a potential sweep from 1 to 1.6 V vs. RHE at a scan rate of 10 mV s^{-1}.

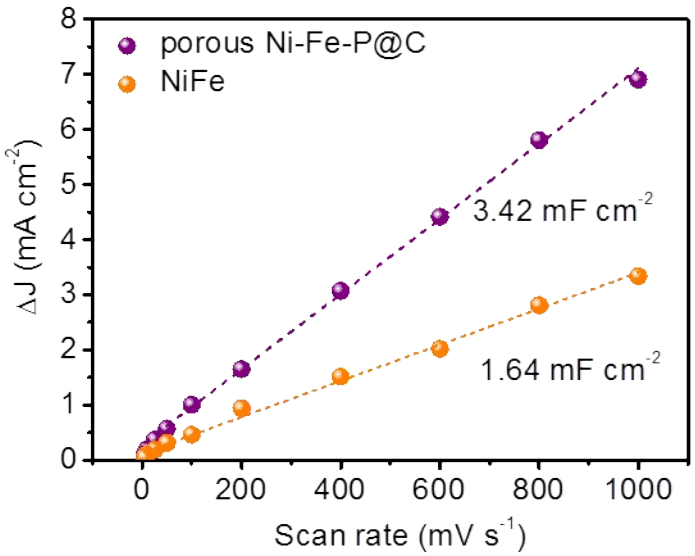

Fig. S13 Capacitive J versus scan rate for NiFe and porous Ni-Fe-P@C NRs. The linear slope corresponds to twice of the double-layer capacitance (C_{dl}).

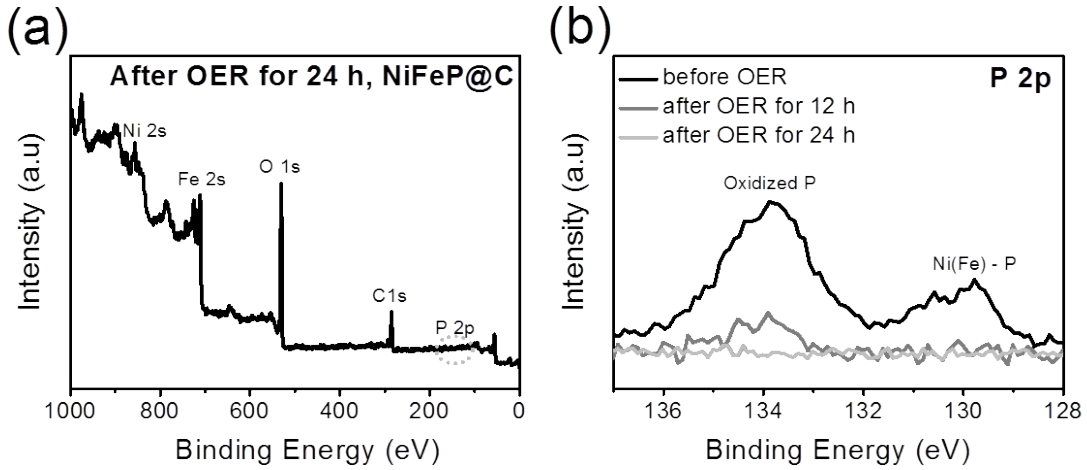

Fig. S14 (a) Overall XPS analysis of Ni-Fe-P@C NRs after the oxygen evolution reaction at 10 mA cm^{-2} for 24 h, (b) P 2p spectrum of Ni-Fe-P@C before and after the oxygen evolution reaction at 10 mA cm^{-2} for 12 h and 24 h.

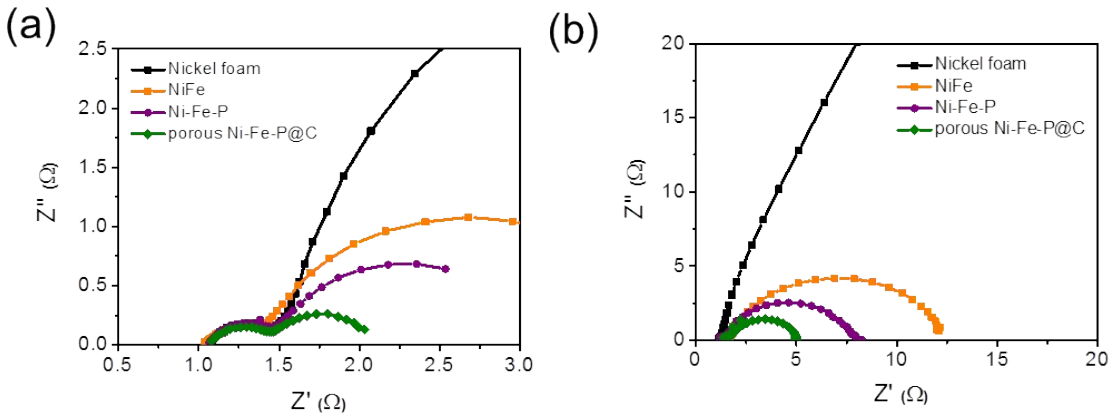

Fig. S15 Nyquist plots obtained from the EIS analysis for the as-prepared catalyst in (a) HER region with an overpotential of 100 mV and (b) OER region with an overpotential of 250 mV in N_2-bubbled 1 M KOH solution.

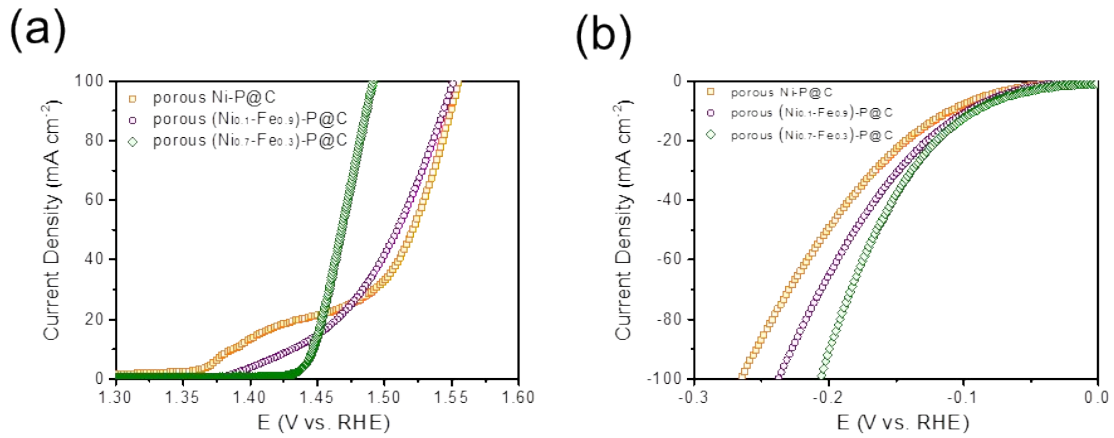

Fig. S16 Linear sweep voltammetry (LSV) curves of the MOF-treated catalysts towards (a) OER and (b) HER in N_2-saturated 1 M KOH solution at 1 mV s^{-1}.

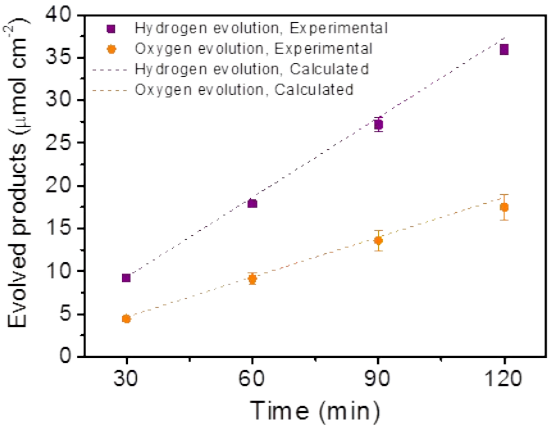

Fig. S17. The calculated and actual gas production by the overall water splitting with Ni-Fe-P@C as a bi-functional catalyst in 1 M KOH solution at 10 mA cm^{-2} in a 2-electrode configuration.